Gateway mechanism confers ultrasensitivity on motor's function

Oshri Afanzar[1†], Diana Di Paolo[2], Miriam Eisenstein[3], Kohava Levi[1], Anne Plochowietz[2], Achillefs N. Kapanidis[2], Richard Michael Berry[2] and Michael Eisenbach[1*]

[1]Department of Biomolecular Sciences, The Weizmann Institute of Science, 7610001 Rehovot, Israel

[2]Biological Physics Research Group, Clarendon Laboratory, Department of Physics, University of Oxford, Oxford, UK

[3]Department of Chemical Research Support, The Weizmann Institute of Science, 7610001 Rehovot, Israel

* To whom correspondence should be addressed. Email m.eisenbach@weizmann.ac.il.

Summary

In bacteria such as *Escherichia coli*, information from the chemotaxis system to the flagellar motor is transduced by a single protein, CheY. The motor responds to CheY by switching its direction of rotation from the default direction to the other. This response is ultrasensitive, but the mechanism underlying this ultrasensitive switching is unknown. Here we resolved this mechanism. We show that the motor employs three sequential steps of CheY binding to distinct sites at the motor, each with a different outcome. Binding to the first site activates CheY at the motor. Binding to the second site generates transient motor switching and enables binding to the third site, which stabilizes the switched state. We demonstrate by mathematical modeling that such a gateway mechanism provides ultrasensitivity. The unique combination of tight regulation and flexibility provided by this mechanism raises the possibility that similar mechanisms may be functional in other systems as well.

† Present address: Department of Chemical and Systems Biology, Stanford University, Stanford, CA 94305, USA

Keywords

Bacterial chemotaxis, bacterial flagellar motor, CheY, flagellar rotation, flagellar motor, flagellar switch.

Introduction

Chemotaxis of bacteria is achieved by modulating the direction of flagellar rotation. This is done by a switch — a large complex at the base of the flagellar motor, consisting of multiple copies of the proteins FliM, FliN and FliG (Figure 1A). In bacteria like *Escherichia coli*, the switch shifts the direction of rotation from the default, counterclockwise, to clockwise in response to binding the signaling protein CheY, which shuttles back and forth between the chemotaxis receptor complex and the flagellar motor. CheY can be activated by phosphorylation to generate clockwise rotation. This activation is regulated by CheA and CheZ as specific kinase and phosphatase, respectively (Figure 1B). A receptor-mediated attractant response (or removal of a repellent) inhibits CheA activity; stimulation by repellents (or attractant removal) enhances its activity (for reviews — [1-4]). Another covalent modification that activates CheY to generate clockwise rotation is lysine-acetylation [5-7]. The regulation of acetylation is known to involve Acs and CobB as acetyl-transferase and deacetylase, respectively (Figure 1B) [8,9]. It is not known whether other components are involved in regulation of CheY acetylation and what role acetylation plays in bacterial chemotaxis [10].

Earlier studies of the corresponding author's group revealed that phosphorylated CheY (CheY~P) mainly binds to the motor at the *N*-terminus of FliM ($FliM_N$) [11,12]. Subsequently, two additional sites with weaker binding of CheY were reported (termed hereafter 'low-affinity sites'), one at FliN, to which the binding is $FliM_N$-dependent [13], and one at FliM at other location than $FliM_N$ [14]. CheY binding to $FliM_N$ [11,12,15,16] and, apparently to FliN [13], is regulated by phosphorylation. NMR analysis in *Thermotoga maritima* identified the middle domain of FliM ($FliM_M$) as a low-affinity binding site for CheY [17], suggesting that similar binding may also occur in *E. coli*.

The motor response to CheY binding is ultrasensitive, meaning that the dependence of clockwise generation on CheY concentration is highly cooperative [18]. The mechanism underlying this ultrasensitivity is unknown and, as a matter of fact, it is quite intriguing in view of the observation that CheY binding to the motor is non-cooperative [19,20].

Each cell contains multiple flagellar motors. When a considerable fraction of flagella rotate clockwise, the cell preforms a vigor turning motion termed tumbling [21,22], as a result of which the subsequent linear swimming is in a randomly

new direction. It was proposed [23] and demonstrated [24] that anisotropic tumbling (in which only some of the motors rotate clockwise for a very short time), does not randomize the swimming direction and maintains directional persistence of swimming. This behavior was proposed to markedly improve the performance of collective migration [24], implying an evolutionary advantage. Maintenance of directional persistence requires extremely short intervals of clockwise rotation. It is unclear how an ultrasensitive motor can produce relatively long clockwise intervals for tumbling and short intervals for directional persistence.

The questions raised above are essentially parts of a wider question — how the motor switches from one direction of rotation to another. Indeed, in spite of decades of studies of the motor's function, the molecular mechanism underlying switching has remained obscure. Suspecting that one of the reasons for this situation is the inability of earlier studies to distinguish between the functions of each of the individual CheY-binding sites at the switch (due to the masking effect of the high-affinity binding of CheY to $FliM_N$), we commenced a study aimed at revealing the functions of each of these sites.

Results

CheY binding to the motor's low-affinity sites generates clockwise rotation

To determine whether CheY binding to the low-affinity sites is functional and physiologically relevant, we investigated the binding and functional interaction of CheY with motors in which FliM had been truncated to remove $FliM_N$ (termed hereafter $FliM_{\Delta N}$), which contains the high-affinity CheY-binding site. To study binding, we employed *in vivo* Förster resonance energy transfer (FRET). We measured the interaction between overexpressed CheY-mCherry and $FliM_{\Delta N}$-YPet-labeled motors, using a Δ*cheZ* background to ensure that CheY-mCherry was mostly phosphorylated (Figure 1C for an explanatory scheme; Figure S1 for a detailed representative analysis). Addition and subsequent removal of the attractant serine caused reduction or enhancement, respectively, of the FRET signal, implying the interaction of CheY-mCherry with the low-affinity sites (Figure 1D, blue). The amplitude of this response was similar to that of non-truncated FliM (termed hereafter $FliM_{wt}$)-YPet motors (Figure 1D, red). Nevertheless, the response was slower in $FliM_{\Delta N}$ cells, and the CheY-mCherry concentration had to be an order of magnitude higher in the case of $FliM_{\Delta N}$ cells (~170 μM vs. ~15 μM in $FliM_{\Delta N}$ and $FliM_{wt}$ cells, respectively). The response of CheY-mCherry under conditions that do not allow its phosphorylation (Δ*cheA* background, i.e., the kinase is missing and the phosphatase is present) was complex and smaller in amplitude (Figure 1D, yellow). No response was observed in a negative control with

103 overexpressed mCherry (Figure 1D, purple). To determine whether this binding to
104 the low-affinity sites is functional, we examined whether it can generate clockwise
105 rotation of the motor. We tethered cells containing $FliM_{\Delta N}$-YPet motors and ~100
106 μM CheY in a Δ*cheZ* background (to ensure phosphorylation of CheY) to glass via
107 their flagella (Figure 1E), and analyzed their direction of rotation with an automated
108 home-made software. The cells responded to positive stimuli (attractant addition
109 or repellent removal) with reduced clockwise rotation (Figure 1F). Repellent
110 stimulation had hardly any effect in this background (Figure 1G). CheY acetylation,
111 stimulated by the acetyl donor acetate, also generated clockwise rotation in $FliM_{\Delta N}$
112 cells (Figure 1H, blue). It is worth noting that the decrease in clockwise level in
113 response to acetate removal was biphasic. Although acetate also functions as a
114 repellent, the clockwise generation was the outcome of acetylation because the
115 repellent benzoate, which acts as a repellent by the same mechanism as does
116 acetate [25,26] but does not serve as an acetyl donor [6,8], did not generate clockwise
117 rotation (Figure 1H, red; Figure S4 for sequential additions of acetate and other
118 repellents). These results suggest that CheY binding to the low-affinity sites is
119 functional in the sense of generating clockwise rotation, and that acetylation is
120 apparently more potent than phosphorylation for this.

121 **$FliM_N$ filters CheY from the cytoplasm and activates it**

122 The finding that $FliM_N$ is not essential for clockwise generation raised the question
123 of what its role is. $FliM_N$ promotes the interaction of CheY with the motor because,
124 in its absence, CheY must be overexpressed for clockwise generation. Therefore,
125 a reasonable possibility is that $FliM_N$ tethers CheY to the motor, thereby elevating
126 the local concentration of CheY at the low-affinity sites [13,17]. According to this
127 possibility, $FliM_N$ acts as a 'fishing line', increasing the rate of CheY association
128 with the clockwise-generating low-affinity sites at the motor. However, this might
129 not be the only function of $FliM_N$. It has been found that $FliM_N$-bound CheY adopts
130 an intermediate conformation between the active and inactive states [27] and
131 enhances the rate of CheY phosphorylation by small phosphodonors [28]. This begs
132 the question of whether these observed features serve to increase CheY's potency
133 to generate clockwise rotation when it is tethered to $FliM_N$. To examine this
134 possibility, we studied the motor behavior in a $FliM_{\Delta N}$ strain that expresses CheY
135 fused to $FliM_N$ ($FliM_N$–CheY) and compared it with the motor's behavior of the same
136 strain that expresses wild-type CheY instead of $FliM_N$–CheY. The expression of
137 both proteins was induced in parallel and under identical conditions to different
138 levels by an IPTG-inducible promoter. We made this comparison in Δ*cheZ* and
139 Δ*cheA* backgrounds, elevating and lowering CheY phosphorylation, respectively.
140 In a Δ*cheZ* background, cells expressing $FliM_N$–CheY~P spent much more time in
141 clockwise rotation than cells expressing CheY~P (Figure 2A; blue and red,

142 respectively). In Δ*cheA* background, cells expressing $FliM_N$–CheY could generate
143 low levels of clockwise rotation whereas cells expressing wild-type CheY could not
144 produce clockwise rotation (Figure 2A, B; cyan and purple, respectively). This
145 implies that CheY can acquire an active clockwise-generating conformation as a
146 result of binding to $FliM_N$. Acetylation, mediated by saturating concentrations of
147 acetate, greatly enhanced clockwise rotation (Figure 2A-B; green). The response
148 of the cells was sigmoidal with respect to acetate concentration (Figure 2C for
149 responses and Figure 2D for summarized response curve). The reason for this
150 sigmoidity is unclear. The cooperative deactivation of Acs by PatZ-mediated
151 acetylation [29] could be a reason this sigmoidity, provided that Acs acetylation
152 inhibits the conversion of acetate to AcAMP but not the subsequent conversion of
153 AcAMP to AcCoA. The response to acetate removal was monophasic at low
154 acetate concentrations but biphasic at high concentrations (Figure 2C; black lines).
155 This biphasic response to acetate removal in cells expressing $FliM_N$–CheY differed
156 from the cognate biphasic response in cells expressing non-modified CheY (Figure
157 1H) in the sense that here, contrary to CheY-expressing cells, the slow phase
158 preceded the rapid one. This difference implies that the biphasic response is not
159 due to acetate metabolism. The clockwise-generating effect of acetate was
160 acetylation specific as benzoate had no effect on the clockwise rotation (Figure
161 2E). Notably, at high $FliM_N$-CheY levels, both stimulus types, attractants and
162 repellents, caused reduced clockwise rotation. However, unlike the response to
163 benzoate and leucine, which started as a repellent response and then reversed,
164 the response to acetate was clockwise elevation from the very beginning (Figure
165 2F). The inverted repellent response observed herein at high $FliM_N$-CheY
166 concentration resembles the inverted attractant response reported for CheY-
167 containing gutted *E. coli* cells [30].

168 To substantiate the conclusion that $FliM_N$ activates CheY independently of
169 phosphorylation, we took advantage of CheY(D13K) being a constitutively active
170 non-phosphorylatable variant of CheY [31] and compared its dose-dependent
171 clockwise-generating activity with that of $FliM_N$-CheY(D13K) in Δ*cheA* background.
172 The $FliM_N$ fusion extremely increased the clockwise generation potency of
173 CheY(D13K) (Figure 2G), so much so that clockwise rotation could be generated
174 without induction, just by the leaky expression of the protein from the plasmid.
175 Leaky expression levels were roughly equivalent to endogenous CheY expression
176 levels, suggesting that, with respect to the CheY concentration required for
177 clockwise generation, the $FliM_N$ fusion to CheY(D13K) substantially compensated
178 for the $FliM_N$ deletion from the motor. This strongly supports the notion that $FliM_N$
179 functions to promote switching in a phosphorylation-independent manner.

180 Taken together, the results suggest that $FliM_N$ not only tethers CheY to the
181 motor but also activates it, and that phosphorylation and acetylation further

182 enhance this activation. However, high CheY~P-FliM$_N$ levels result in an inverted
183 response. Another function suggested for FliM$_N$ was to provide some of the
184 interface required for the interaction of CheY~P with FliN [13]. While our results do
185 not test the validity of this suggestion, it should be noted that this function is
186 phosphorylation dependent whereas the function of FliM$_N$, demonstrated herein,
187 appears to be phosphorylation independent.

188 **Both CheY binding and clockwise generation are biphasic processes**

189 Clockwise generation in the absence of FliM$_N$ indicates that one or more of the
190 other CheY-binding sites, i.e., of the low-affinity sites, is involved in CheY binding.
191 The way that CheY interacts with these sites is of special interest in view of the
192 fact that the motor's response to CheY is ultrasensitive [18] even though the binding
193 of CheY to the motor is non-cooperative [19,20]. Since these published binding
194 experiments essentially reflected binding to the high-affinity site at FliM$_N$, we
195 investigated whether CheY binding to the low-affinity sites is cooperative and, if
196 so, whether it can explain the ultrasensitive response of the motor. To this end, we
197 measured the amount of CheY bound to FliM$_{\Delta N}$ motors as a function of the
198 intracellular concentration of CheY. We determined the amount of bound CheY by
199 FRET photobleaching, measuring the increase in fluorescence intensity of the
200 donor, FliM$_{\Delta N}$-YPet, due to photobleaching of the acceptor, CheY~P-mCherry
201 (Figure 3A, B). This technique was used previously for FRET measurements of
202 chemotactic signaling at the population level [32]. We preformed the measurements
203 *in vivo*, in single cells, using a Δ*cheZ* background to promote CheY
204 phosphorylation (Figure 3C, black curve, for one representative experiment out of
205 three). We used parallel measurements with free mCherry to control for non-
206 specific binding (Figure 3C, purple curve). We found that, in all measurements, the
207 fitted binding curve could be described as the sum of two binding processes
208 (Figure 3D; black for the average fitted curve of three experiments; red and blue
209 for the binding processes derived from this black binding curve). It appears that a
210 saturation process was predominant at low CheY concentrations and a
211 cooperative-like process was dominant at high concentrations. It should be noted
212 that none of the measured FRET phases was due to FRET signals between free
213 FliM$_{\Delta N}$-YPet and CheY-mCherry molecules in the cytoplasm. This is for two
214 reasons. First, no CheY~P-mCherry binding to FliM$_{\Delta N}$-YPet was detected *in vitro*
215 at these CheY concentrations. And second, only spots of high intensity FliM$_{\Delta N}$-
216 YPet signal were measured. Likewise, the non-cooperative and cooperative
217 binding phases were not due to CheY~P-mCherry binding to FliM$_{\Delta N}$-YPet in the
218 cytoplasm and in the motor, respectively. This is because clockwise rotation could
219 be observed at CheY concentrations lower than those of the cooperative phase. If

220 only the latter contributed to CheY binding to the motor, clockwise rotation could
221 not have been observed.

222 Two CheY-binding phases, as found above, may well give rise to a biphasic
223 motor response to CheY, meaning that the outcome of each binding phase is a
224 different clockwise-generation mechanism. If so, there is a good chance that the
225 clockwise intervals generated by each mechanism would be distributed around a
226 different interval length. Furthermore, because each of the binding phases occurs
227 at a different concentration range of CheY (Figure 3D) and because the extent of
228 clockwise rotation is dependent on the intracellular CheY concentration (Figure
229 2A), we expected that the clockwise distribution related to each mechanism would
230 be dependent on the clockwise level. To put all these to the test, we measured the
231 lengths of clockwise intervals in $FliM_{\Delta N}$ motors and studied their distributions at
232 different clockwise levels.

233 We quantified switching by video analysis of tethered Δ*cheA* cells
234 containing $FliM_{\Delta N}$ motors and expressing $FliM_N$-CheY in the presence of acetate
235 (10 mM, pH 7.0), recorded at 75 frames/s. We defined clockwise intervals as
236 intervals that have at least 4 consecutive frames (52 ms) of clockwise rotation at a
237 rate higher than 1 Hz, which is the measured rotation rate of fluctuations of non-
238 rotating cells distributed around 0±0.5 Hz (±SD). This 4-frame threshold excluded
239 short events that might not be clockwise rotation mediated by CheY. This is
240 according to a negative control consisting of a Δ*cheY* strain, in which the
241 generation of clockwise rotation cannot be mediated by CheY. In this negative-
242 control strain we studied 1 min recordings of 344 cells, and found ~100 clockwise
243 intervals, all shorter than 50 ms. Figure 4A shows an example of a clockwise
244 interval lasting 4 frames, the shortest duration that exceeded the threshold (see
245 also supplementary Movie S1). To avoid artefacts that might have been caused by
246 interactions between the cell body and the surface, we also excluded from the
247 analysis intervals that were flanked by pause events (Figure 4B; pause events
248 were defined as absolute rotation rate <1 Hz for more than 2 consecutive frames).
249 We grouped clockwise intervals from cells that had similar average clockwise
250 levels and produced from each group a distribution of interval lengths (Figure 4C).
251 At low clockwise levels, the distribution appeared as a fast, monophasic
252 exponential decay (Figure 4C, blue; note the logarithmic scale of the ordinate, in
253 which exponential decays are seen as straight lines). The distribution became
254 biphasic at intermediate clockwise levels (Figure 4C, gray), and slow monophasic
255 at high clockwise levels (Figure 4C, orange). To calculate the contribution of each
256 of the phases to clockwise rotation time, we fitted each of the distributions in Figure
257 4C with a biexponential expression, and extracted the average time of clockwise
258 rotation of each process in each clockwise level (Figure 4D for demonstration of a
259 calculation for a given clockwise level). Like the first phase of CheY binding to the

motor (Figure 3D), the first phase of clockwise generation steadily increased in clockwise rotation time up to saturation, generating only very short intervals of clockwise rotation (Figure 4E, blue). Like the second binding phase, the second clockwise-generation phase emerged at intermediate clockwise levels, producing long intervals of clockwise rotation (Figure 4E, red). The average reversal frequency of these motors was roughly 8-fold higher than that of wild-type motors (Figure 4F compared with peak reversal frequency of ~0.8 s^{-1} in wild-type cells containing constitutively active CheY [33]), meaning overall shorter clockwise intervals. This difference is probably a reflection of the lower affinity of $FliM_{\Delta N}$ motors for CheY relative to that of motors containing $FliM_{wt}$. These results suggest that the two phases of CheY binding to the motor bring about two phases of clockwise generation.

The measurements above (Figure 4C-F) were based on motors of cells in which acetylation of CheY was promoted. We verified that similar distributions were obtained when CheY was activated by phosphorylation, by D13K mutation, and by $FliM_N$ fusion (Figure S5), meaning that the biphasic motor response was not the product of acetylation dynamics. Interestingly, when clockwise rotation was generated by $FliM_N$-CheY (in the absence of any other activation), only short intervals were observed (Figure S5B). This observation taken together with the limited clockwise-generation activity of this variant (Figure 2A, cyan) suggests that the generation of the second phase depends on excessive CheY activation. Thus, it appears that adequate CheY activation is required for the formation of a biphasic response.

The first phase of clockwise generation enables directional persistence in swimming

Since the first clockwise-generation phase was characterized by very brief clockwise intervals (Figure 4E, blue), and since generation of such short intervals only slightly deflects the swimming trajectory and maintains directional persistence [23,24], we investigated whether the first clockwise-generation phase indeed preserves directional persistence. We assessed the distribution of angular deflection in swimming cells, with an expectation to find that the distribution peaks at small turning angles, compatible with directional persistence. For this, we measured the angular shift in 1 s trajectories of *fliM*$_{\Delta N}$ Δ*cheA* cells expressing $FliM_N$-CheY in the absence or presence of acetate (Figure S6; blue and red, respectively). As a control for noise, we made similar measurements in cells that do not express CheY and, therefore, do not tumble (Figure S6; green and purple for the absence or presence of acetate, respectively). The experimental distributions were significantly different from the control distributions ($P = 6\times10^{-9}$ and 4×10^{-26} for the absence and presence of acetate, respectively, according to a

299 two-sample Kolmogorov-Smirnov test). In the absence of CheY, turning angles
300 can be related to noise. The same noise is expected to appear also in the
301 experimental distributions. To de-noise the experimental distributions, we
302 subtracted them from the control distributions (Figure 4G). We found that both in
303 the absence or presence of acetate, the subtracted distribution peaked at 20°
304 (Figure 4G), which is the angular deflection expected to maintain directional
305 persistence of swimming. It is worth noting that, under some assumptions, a peak
306 distribution of 20° turning angle was calculated to be the product of an average
307 clockwise intervals of 50 ms [34]. This value is approximately the average clockwise
308 interval length of the first phase of clockwise generation in our measurements
309 (Figure 4E and Figure S5B). Thus, the first phase of clockwise generation appears
310 to produce angular deflection while maintaining directional persistence. Somewhat
311 larger proportion of high deflection angles were observed in the presence of
312 acetate, suggesting that acetate is less supportive of directional persistence.

313 **CheY binding to FliN is apparently responsible for the first phase of**
314 **clockwise generation**

315 The simplest explanation of biphasic binding that results in biphasic clockwise
316 generation is CheY binding to two different sites on FliM$_{\Delta N}$ motors. Since, as
317 mentioned above, the known CheY-binding sites in FliM$_{\Delta N}$ motors are the low-
318 affinity sites at FliN and FliM$_{M}$, we determined whether or not this explanation is
319 correct by studying the generation of clockwise rotation in a *fliN*(A93D) mutant, in
320 which the interaction of FliM$_{N}$-CheY~P with FliN is greatly impaired [13]. We
321 expected that if CheY indeed binds to two different motor sites, the distribution of
322 interval lengths would be skewed by the FliN mutation. To this end, we first
323 characterized how FliM$_{N}$-CheY affects clockwise generation in the mutant. We
324 found that clockwise generation by FliM$_{N}$-CheY~P was highly impaired in the
325 *fliN*(A93D) mutant (Figure 4H, blue), supporting the conclusion of Sarkar *et al.* [13]
326 that FliN is involved in FliM$_{N}$-CheY~P binding. Pushing phosphorylation further by
327 the repellent benzoate did not increase clockwise rotation (Figure 4H, red point).
328 Unlike phosphorylation, FliM$_{N}$-CheY acetylation and, the more so, acetylation and
329 phosphorylation together, led to significant clockwise rotation (Figure 4H, green
330 and purple, respectively). To determine whether the *fliN*(A93D) mutation affected
331 any of the switching phases, we calculated the distributions of clockwise interval
332 length of the mutant under phosphorylating and acetylating conditions (Δ*cheZ*
333 background in the presence of acetate). As in the case of non-mutated FliN, two
334 phases of clockwise generation were observed (Figure 4I). However, the first
335 clockwise-generation phase was saturated already at the lowest clockwise level
336 (Figure 4J, blue) along with the emergence of the second phase (Figure 4J, red),
337 and very short intervals of clockwise rotation were hardly observable (Figure 4I).

338 Similar observations were made when the cells lacked CheA (in which only
339 acetylation occurred; Figure 4K), suggesting that the generation of long intervals
340 were the result of CheY acetylation. The occurrence of long intervals could also be
341 demonstrated by the peak reversal frequency of these motors, which was roughly
342 3-fold lower than that of wild-type $FliM_{\Delta N}$ motors (Figure 4L; cf. Figure 4G). This
343 implies that short intervals of clockwise rotation, manifested as frequent reversals,
344 are associated with CheY binding to FliN, and long intervals, manifested as low
345 reversal frequency, is mostly dependent on CheY binding to another site.

346 **CheY binding to $FliM_M$ is apparently responsible for the second phase of**
347 **clockwise generation**

348 The suppression of short intervals of clockwise rotation when CheY interaction with
349 FliN was impaired strongly suggested that long intervals are produced by CheY
350 interaction with a motor site other than FliN. An obvious candidate site for this
351 binding is the other low-affinity binding site, $FliM_M$, shown to bind CheY in *T.*
352 *maritima* [17]. To examine the plausibility of CheY binding to $FliM_M$ in *E. coli*, we
353 employed *in vivo* crosslinking of cells expressing $FliM_{\Delta N}$-YPet, using a non-specific
354 crosslinker, glutaraldehyde. (We wish to point out that FRET experiments *in vivo*
355 cannot distinguish CheY binding to FliM from CheY binding to FliN due to the
356 physical proximity of FliM to FliN.) The advantage of using crosslinking is that,
357 beyond being carried out *in vivo*, it can detect weak interactions. We tracked the
358 crosslinking products by SDS-PAGE and scanning the gel for $FliM_{\Delta N}$-YPet
359 fluorescence. This enabled us to quantify the extent of complex formation. Among
360 many other crosslinking products, we obtained a product at the size of a complex
361 between $FliM_{\Delta N}$-YPet and CheY (Figure 5A, lanes 1–3). The formation of this
362 complex was dependent on CheY overexpression (Figure S7), implying that the
363 complex indeed contained CheY. These observations are consistent with the
364 possibility of CheY binding to $FliM_M$ *in vivo*, but they do not rule out a possibility of
365 CheY binding to another FliM domain (e.g., to the C terminus domain of FliM).
366 Various direct *in vitro* binding assays between purified CheY and $FliM_{\Delta N}$ were not
367 conclusive, probably due to the low affinity of $FliM_{\Delta N}$ for CheY.

368 To examine the likelihood that CheY binding to $FliM_M$ is functional, we
369 employed docking analysis between CheY and $FliM_M$ based on their binding
370 interface in *T. maritima* (Supplementary Methods for detailed description). We
371 especially paid attention to the β4α4 loop of CheY, known to be at the CheY-$FliM_M$
372 binding interface in *T. maritima* [17] and predicted in our earlier all-atom molecular
373 dynamics simulation to be activated by CheY acetylation at its clockwise-
374 generating site Lys-91 [35]. In the docking analysis, we produced a number of
375 models of CheY binding to $FliM_M$ in *T. maritima*, and translated those fitted well
376 with the NMR results of Dyer *et al*. [17] to *E. coli* proteins by superposing the active

377 and inactive forms of CheY upon the model of $FliM_M$. We substantiated the
378 superposition results by docking the *E. coli* proteins independently of the *T.*
379 *maritima* model. This docking demonstrated that while the active conformation of
380 CheY well docked onto $FliM_M$ (Figure 5B, up-left docking model), the inactive
381 conformation of the $\beta4\alpha4$ loop of CheY clashed with $FliM_M$ (Figure 5B, down-right).
382 This is consistent with the proposition that acetylation generates clockwise rotation
383 by enhancing the binding of CheY to $FliM_M$, and that this enhancement is done by
384 modulation of the $\beta4\alpha4$ conformation.

385 The analysis predicted two prominent latching interfaces of CheY with
386 $FliM_M$. One interface is electrostatic and is mostly contributed by arginine at
387 position 94 of FliM (Figure S8A). The other interface is a hydrophobic patch in FliM
388 (Figure S8B). To determine the functional relevance of the first interface, we
389 examined the rotation of motors of cells expressing $FliM_{\Delta N}$(R94S) or $FliM_{\Delta N}$(R94L)
390 in a Δ*cheZ* background and overexpressing $FliM_N$-CheY. These motors hardly
391 rotated clockwise even when benzoate was used to further stimulate CheY
392 phosphorylation. Very low levels of clockwise rotation were observed following the
393 promotion of CheY acetylation by acetate (Figure 5C). These results are in line
394 with the docking model's prediction that FliM(R94) is involved in CheY binding. To
395 determine the functional relevance of the second interface, we examined whether
396 replacement of a charged residue to a hydrophobic one within the hydrophobic
397 CheY-$FliM_M$ binding interface (E214W) would increase clockwise generation.
398 Indeed, clockwise rotation in the *fliM*$_{\Delta N}$(E214W) mutant in a Δ*cheZ* background
399 was observed at much lower $FliM_N$-CheY expression levels (Figure 5D). It appears
400 that the mutation affected the motor's sensitivity to CheY rather than affecting its
401 intrinsic clockwise level because the clockwise rotation levels of *fliM*$_{\Delta N}$(E214W) in
402 a Δ*cheA* background, where $FliM_N$-CheY is mostly inactive and does not contribute
403 much to clockwise generation, were low and comparable to cells containing non-
404 mutated $FliM_{\Delta N}$ (Figure S9; blue). Nevertheless, when $FliM_N$-CheY was activated
405 by acetate, the response of cells with $FliM_{\Delta N}$(E214W) motors exceeded that of
406 $FliM_{\Delta N}$ (Figure S9; red).

407 To determine whether the proposed interaction of CheY with $FliM_M$ affects
408 the second phase of clockwise generation, we examined the distributions of
409 clockwise interval lengths and reversal frequency in *fliM*$_{\Delta N}$(R94SL) and
410 *fliM*$_{\Delta N}$(E214W) mutants. Indeed, only the first phase of clockwise generation was
411 apparent in *fliM*$_{\Delta N}$(R94SL) mutants (Figure 5E, F). The peak reversal frequency of
412 the mutants was roughly similar to that of its wild-type $FliM_{\Delta N}$ parent but the
413 mutants did not reach high clockwise levels (Figure 5G). The distributions of
414 clockwise intervals produced by $FliM_{\Delta N}$(E214W) motors were approximately
415 monophasic at all clockwise levels (Figure 5I), with interval lengths very similar to

416 those exhibited by FliN(A93D) motors (Figure 5J *versus* Figure 4J). Consistently,
417 the peak reversal frequency of the $FliM_{\Delta N}$(E214W) motors was between the values
418 of wild-type $FliM_{\Delta N}$ motors and FliN(A93D) $FliM_{\Delta N}$ motors (Figure 5K *versus* Figure
419 4F, L). It appears that the E214W mutation increased the affinity of $FliM_M$ for CheY
420 to a level higher than that of FliN for CheY. Consequently, intervals initiated by
421 CheY binding to FliN were immediately extended by subsequent binding to $FliM_M$.
422 Furthermore, the inability of the *fliM*$_{\Delta N}$(R94SL) mutant to exhibit long clockwise
423 intervals suggests that CheY binding to $FliM_M$ is required for stable clockwise
424 rotation.

425 Another observation made in these experiments is that the rotation rate in
426 the clockwise intervals was lower in the *fliM*$_{\Delta N}$(R94SL) mutant (Figure 5H) relative
427 to the *fliM*$_{\Delta N}$(E214W) mutant (Figure 5L) and the wild-type $FliM_{\Delta N}$ parent (Figure
428 S5). Notably, the distribution of clockwise rotation rates as well as the distribution
429 of clockwise interval lengths of the *fliM*$_{\Delta N}$(R94SL) mutant (Figure 5H, E) expressing
430 $FliM_N$-CheY under phosphorylating conditions were similar to those of non-mutated
431 $FliM_{\Delta N}$ cells (Figure S5B). Low clockwise rotation rates in motors that are not stably
432 rotating clockwise is consistent with a conformational spread model [36], where low
433 clockwise rotation rate is suggestive of incomplete switching events (i.e., events in
434 which the conformation of the motor did not stabilize in a coherent clockwise
435 conformation). Taken together, these results suggest that the second phase of
436 switching is due to CheY interaction with $FliM_M$, and that the outcome of this
437 interaction is stabilization of the rotation in the clockwise direction.

438 **CheY~P and CheY~Ac preferentially bind to FliN and $FliM_M$, respectively**

439 The observation that clockwise generation in FliN(A93D) motors could only be
440 observed in the presence of acetate (Figure 4H) raised the possibility that the low-
441 affinity binding sites have different preferences for CheY~P and for CheY~Ac. To
442 examine this possibility, we first investigated whether CheY~P and CheY~Ac have
443 different *in vivo* affinities for the motor. To this end, we compared *in vivo* the dwell
444 time of single CheY molecules at FliM-YPet motors between phosphorylating
445 conditions, acetylating conditions, and conditions under which CheY is both
446 phosphorylated and acetylated. We electroporated CheY(I95V) molecules labeled
447 with a maleimide modification of the photo-stable organic dye Atto647 into FliM-
448 YPet expressing cells [37]. The experiments were carried out both in a Δ*cheZ*
449 background to make CheY fully phosphorylated and in a Δ*cheA* background to
450 make CheY non-phosphorylated. The *cheY*(I95V) mutation was designed to
451 increase CheY affinity for $FliM_N$ [38], thus enhancing sampling of otherwise rare
452 binding events. Custom-written software tracked CheY(I95V)-Atto647 molecules
453 and estimated motor locations in each cell using FliM-YPet fluorescence images.
454 CheY(I95V)-Atto647 molecules dwelling within 75 nm of a motor for >30 ms were

455 interpreted as binding to the motor (Figure 6A; see Methods). Presence of acetate
456 increased the dwell time of CheY at the motor (Figure 6B and 6C for the survival
457 probabilities of CheY~P and CheY, respectively, to remain bound to the motor;
458 Movie S2). Notably, the very long dwell events in Movie S2 were only detected in
459 the presence of acetate. The extension of CheY's dwell time at the motor by
460 acetylation taken together with the generation of long clockwise intervals by
461 acetate even when CheY binding to FliN is impaired (Figure 4I) suggest that $FliM_M$
462 has a preference for CheY~Ac.

463 To examine whether, indeed, CheY~P and CheY~Ac preferentially bind to
464 FliN and $FliM_M$, respectively, we measured the concentration-dependent response
465 of $FliM_{\Delta N}$ motors to CheY~P, CheY~Ac, and CheY with both modifications
466 combined, expecting to observe concentration dependence that resembles the two
467 phases of CheY binding to the motor (Figure 3D). Unmodified CheY did not
468 produce clockwise rotation (pre-acetate stimulation in Figure 6D; purple curve in
469 Figure 6F). CheY acetylation achieved by acetate addition increased, after a short
470 delay, the fraction of time spent in clockwise rotation (Figure 6D). The extent of the
471 response was sigmoidally dependent on the CheY level (Figure 6F, red).
472 Increasing concentrations of CheY~P (CheY in a Δ*cheZ* background) enhanced
473 clockwise rotation up to saturation (Figure 6F, blue). Acetylation of CheY~P further
474 enhanced clockwise rotation (Figure 6E; Figure 6F, green). Notably, the clockwise
475 curve of CheY~P (Figure 6F, blue) resembled the first binding phase (Figure 3D,
476 blue), including the CheY~P concentration required for achieving saturation.
477 Likewise, the clockwise curve of CheY~Ac (Figure 6F, red) resembled the second
478 phase of binding (Figure 3D, red). These resemblances endorse the conclusion
479 that the first binding phase (blue) in Figure 3D is more associated with CheY~P
480 binding and the second phase (red) is mainly associated with CheY~Ac binding.
481 They also suggest that the motor hypersensitivity to CheY is the outcome, at least
482 in part, of the apparently cooperative binding of CheY~Ac and CheY~Ac~P to
483 $FliM_M$ (see Discussion).

484
Discussion

485 The molecular mechanism underlying the motor's switching from one direction of
486 rotation to the other, which is the essence of bacterial chemotaxis, is yet unknown.
487 Here we showed that clockwise generation is mediated by CheY interaction with
488 three different sites at the motor. We revealed the function of each of these sites
489 and the probable sequence of events at the motor during switching from
490 counterclockwise to clockwise rotation.

491 **Functions of $FliM_N$**

492 We found that the first site to which CheY binds, a high-affinity site at $FliM_N$, is not
493 essential for clockwise generation (Figures 1D, 2A). It tethers CheY to the motor
494 and activates it. We propose that this CheY activation at the motor is a preliminary
495 step in the process of clockwise generation (Figure 7A), which may have evolved
496 to filter out crosstalk with proteins having CheY-like topology in other two-
497 component signaling pathways. Binding of such proteins to $FliM_N$ is expected to be
498 futile.

499 **Functions of the other CheY-binding sites in the switching mechanism**

500 We showed that, in $FliM_{\Delta N}$ motors, CheY binding to the motor is biphasic (Figure
501 3D) as a result of binding to two different sites at FliN and $FliM_M$. We further
502 demonstrated that CheY binding to these sites generates short and long clockwise
503 intervals, respectively, reflected in a biphasic clockwise generation (Figures 4–6),
504 and that FliN has preference for CheY~P and $FliM_M$ for CheY~Ac. We propose that
505 CheY~P binding to FliN makes the first catalytic step of clockwise generation,
506 producing mainly brief episodes of clockwise rotation (Figure 7B). CheY~Ac
507 binding to $FliM_M$ makes the second catalytic step of clockwise generation,
508 produces long clockwise intervals and, thereby, stabilizes the rotation in clockwise
509 direction (Figure 7C). Because the conformation of FliM is different in the
510 counterclockwise and clockwise states, it is reasonable that $FliM_M$ can only bind
511 CheY when it is in its clockwise state, meaning that the generation of brief
512 clockwise rotation by the preceding binding step to FliN enables binding to $FliM_M$
513 and generation of longer clockwise rotation. Indeed, when CheY interaction with
514 $FliM_M$ was turned down, the motor produced only short intervals of clockwise
515 rotation (Figure 5E-G) that were relatively slow in rate (Figure 5H), suggesting
516 incomplete switching according to the conformational-spread model [36]. This
517 observation was not captured in earlier attempts to characterize the switching
518 process, probably because of the masking effect of $FliM_N$ in those experiments.
519 The presence of $FliM_N$ is also the reason for earlier findings [9,39] that acetylation
520 reduces the binding of CheY to $FliM_{wt}$ *in vitro*.

521 **Physiological significance**

522 This switching mechanism provides dynamics and flexibility to the system in two
523 senses. First, at the intermediate stage, the system can either proceed to a stable
524 rotation in the new direction or shift back to the original direction. And second, it
525 provides the system flexibility with respect to the swimming patterns. It appears
526 that the first CheY binding phase is associated with swimming patterns that enable
527 slight reorientation while maintaining directional persistence (Figure 4G), and the
528 second phase, which produces long clockwise intervals, results in tumbling events

529 that lead to sharp reorientation. In this way this switching mechanism increases
530 chemotactic performance. With these advantages, it would not be surprising if
531 similar mechanisms are found in the future in the output of other signaling systems
532 as well.

533 **Motor's ultrasensitivity can emerge from a gateway mechanism**

534 The response of wild-type motors to CheY is ultrasensitive [18]. Since CheY binding
535 to $FliM_{wt}$-containing motors is non-cooperative [19,20], meaning that CheY binding to
536 $FliM_N$ does not generate ultrasensitivity, it is conceivable that CheY binding to FliN
537 and $FliM_M$ does generate ultrasensitivity. The question is how. A reasonable
538 possibility is that CheY can only (or mainly) bind to $FliM_M$ when the motor is already
539 rotating clockwise. The finding that FliM subunits within the motor have different
540 orientations in the counterclockwise and clockwise states [40] is consistent with this
541 possibility, as one orientation may sterically block CheY binding. In such a
542 mechanism, which we term a gateway mechanism, clockwise rotation, which
543 results from CheY binding to FliN, exposes another CheY-binding site at $FliM_M$.
544 The binding of CheY to that site stabilizes clockwise rotation. This mechanism is
545 in line with the biphasic curve of CheY binding to the motor (Figure 3D). To
546 examine whether a gateway mechanism can confer ultrasensitivity on the motor's
547 response to CheY, we constructed a simplified kinetic model of the motor in which
548 CheY binds to $FliM_M$ only if FliN is already CheY-bound. The simplified model
549 consists of a single FliN-binding site and two $FliM_M$-binding sites (Figure 8A; the
550 number of binding sites is not expected to affect the conclusion). A requirement
551 from such a model is that the binding affinities of CheY for its binding sites at the
552 motor would affect the ultrasensitivity of the motor. Therefore, we examined CheY
553 binding to the motor as a function of the ratio between CheY affinity for FliN and
554 CheY affinity for $FliM_M$. When the dissociation constant for CheY binding to FliN
555 was much lower than for the binding to $FliM_M$, the modeled binding was
556 multiphasic, but not ultrasensitive (Figure 8B, blue). When the dissociation
557 constant for the binding of CheY for FliN was much higher than for the binding to
558 $FliM_M$, the binding was ultrasensitive (Figure 8B, orange). When the dissociation
559 constants were comparable, the binding was a simple saturation process (Figure
560 8B, gray; note the logarithmic scale). Consistently, the apparent Hill coefficients of
561 the curves shifted from positive cooperativity (Figure 8B, insert, orange), through
562 zero cooperativity (Figure 8 B, insert; grey), to negative cooperativity (Figure 8 B,
563 insert, blue). Thus, ultrasensitivity can arise from a gating mechanism.

564 **Conclusion**

565 The flagellar motor likely binds CheY at a non-catalytic site, $FliM_N$, with a resultant
566 activation of CheY, and at two different catalytic sites, FliN and $FliM_M$, with a

567 resultant generation of short and long intervals of clockwise rotation, respectively.
568 The generation of short and long intervals can support directional persistence and
569 randomization of direction in the tactic behavior of bacteria. Ultrasensitivity in the
570 motor response to CheY may be produced by a gateway mechanism of switching,
571 in which the extent of ultrasensitivity emerges from the difference in affinities of the
572 binding sites for CheY.

573

574 # Methods

575 **Strains and plasmids**

576 To produce *fliM*$_N$ truncation, *fliM-YPet* was cloned from the strain JPA945 [41] (kindly
577 provided by J. Armitage) with genomic flanks of 500 base pairs to the Pst1 sites of
578 pDS132 suicide plasmid [42]. FliM residues 1–16 were truncated from the resulting
579 plasmid by RF-cloning. The constructed plasmid was used to perform allelic
580 exchange with strain JPA945 to produce strain EW566 bearing *fliM*Δ(1-16)-*YPet*
581 genomic mutation. The mutation was verified by PCR sequencing. Plasmidic
582 mutations were produced by RF cloning. The genomic deletion mutations of *cheA*
583 and *cheZ* were produced by subjecting cells to P1 transduction with phage
584 containing the genetic background of strain JW1870 or JW1877, respectively. See
585 Tables S2-3 for detailed strains and plasmids list.

586 **Growth conditions**

587 Strains, diluted 1:100 from overnight cultures, were cultured to mid-late
588 exponential phase at 30°C in tryptone broth with appropriate antibiotics to maintain
589 the plasmids. For CheY expression, cells were grown to mid-late exponential
590 phase and induced by IPTG for 3-4 h. It appeared that dilution of overnight cultures,
591 which spent 1–2 days on the bench at room temperature, produced better
592 responses to acetate.

593 **Analysis of the direction of flagellar rotation**

594 The direction of flagellar rotation was determined by the tethering assay [43].
595 Analysis of the rotation was done automatically by an in-house custom-made
596 MATLAB program. For interval analysis, each subjected interval was considered
597 valid if it was flanked by two other valid intervals or by rotation in the opposite
598 direction. See Supplementary Methods for details and other considerations.

599 **In vivo FRET**

600 Cells were immobilized onto a polylysine-coated 8-well glass bottom (ibidi,
601 Germany), washed 4 times with motility buffer and visualized using an inverted
602 confocal microscope set (IX81, Olympus, Japan) with an UPLSAPO 60x0 NA:1.35
603 objective equipped and excitation lasers at 488 and 559 nm for YPet and mCherry,
604 respectively. FRET was measured by acceptor photobleaching with high intensity
605 559 nm laser. FRET efficiency was estimated as ($I_{Post\ bleaching} - I_{Prior\ bleaching}$) / I_{Post}
606 $_{bleaching}$. See Supplementary Methods for details.

607 **Single molecule analysis**

608 The locations of CheY(I95V)-Atto647 and FliM-YPet were automatically estimated
609 by a custom-made MATLAB script. Motor locations were identified as peaks of
610 fluorescence. The exact motor location was determined by identifying the maxima
611 location of a 2D Gaussian, fitted to each motor spot. For the identification of
612 motors, several images were acquired, normalized and averaged before Atto647
613 imaging. The location of CheY(I95V)-Atto647 was determined similarly to motor
614 location in each frame. CheY(I95V)-Atto647 was considered bound to the motor
615 when it was within 75 nm of a motor location for at least 30 ms (3 frames). Shorter
616 co-localizations were excluded to avoid false positive measurements (e.g.,
617 molecules diffusing near the motor). The value of 30 ms was chosen as the half of
618 the expected mean dwell time of CheY(I95V)-Atto647 with $FliM_N$ [~60 ms given a
619 K_d = 3.9 μM for CheY(I95V)-$FliM_N$ interaction and an estimated $k_{on} = 4x10^6\ M^{-1}s^{-1}$
620 [20,38]]. The mean-square displacement in 2 dimensions due to free diffusion is $<r^2>$
621 $= 4Dt$. Setting $<r^2> = (75\ nm)^2$ and t = 30 ms gives $D = 0.047\ \mu m^2\ s^{-1}$, which is
622 lower than the diffusion coefficient of CheY in the cell. Thus, the false-positive rate
623 due to diffusing molecules is expected to be negligible. See Supplementary
624 Methods for a detailed description of protein labeling and optical setup.

625 ## References

626 1. Berg, H. C. The rotary motor of bacterial flagella. *Annu. Rev. Biochem.* **72,**
627 19–54 (2003).
628 2. Eisenbach, M. in *Chemotaxis* (ed. Eisenbach, M.) 53–215 (Imperial College
629 Press, 2004).
630 3. Terashima, H., Kojima, S. & Homma, M. Flagellar motility in bacteria
631 structure and function of flagellar motor. *Int Rev Cell Mol Biol* **270,** 39–85
632 (2008).
633 4. Porter, S. L., Wadhams, G. H. & Armitage, J. P. Signal processing in
634 complex chemotaxis pathways. *Nature reviews* **9,** 153–165 (2011).
635 5. Wolfe, A. J., Conley, M. P. & Berg, H. C. Acetyladenylate plays a role in
636 controlling the direction of flagellar rotation. *Proc. Natl. Acad. Sci. U.S.A.*
637 **85,** 6711–6715 (1988).

638 6. Barak, R., Welch, M., Yanovsky, A., Oosawa, K. & Eisenbach, M.
639 Acetyladenylate or its derivative acetylates the chemotaxis protein CheY *in*
640 *vitro* and increases its activity at the flagellar switch. *Biochemistry (USA)*
641 **31,** 10099–10107 (1992).
642 7. Barak, R., Abouhamad, W. N. & Eisenbach, M. Both acetate kinase and
643 acetyl Coenzyme A synthetase are involved in acetate-stimulated change
644 in the direction of flagellar rotation in *Escherichia coli*. *J. Bacteriol.* **180,**
645 985–988 (1998).
646 8. Barak, R., Prasad, K., Shainskaya, A., Wolfe, A. J. & Eisenbach, M.
647 Acetylation of the chemotaxis response regulator CheY by acetyl-CoA
648 synthetase from *Escherichia coli*. *J. Mol. Biol.* **342,** 383–401 (2004).
649 9. Li, R. *et al.* CobB regulates *Escherichia coli* chemotaxis by deacetylating
650 the response regulator CheY. *Mol. Microbiol.* **76,** 1162–1174 (2010).
651 10. Barak, R. & Eisenbach, M. Acetylation of the response regulator, CheY, is
652 involved in bacterial chemotaxis. *Mol. Microbiol.* **40,** 731–743 (2001).
653 11. Welch, M., Oosawa, K., Aizawa, S. I. & Eisenbach, M. Phosphorylation-
654 dependent binding of a signal molecule to the flagellar switch of bacteria.
655 *Proc. Natl. Acad. Sci. U.S.A.* **90,** 8787–8791 (1993).
656 12. Bren, A. & Eisenbach, M. The N terminus of the flagellar switch protein,
657 FliM, is the binding domain for the chemotactic response regulator, CheY.
658 *J. Mol. Biol.* **278,** 507–514 (1998).
659 13. Sarkar, M. K., Paul, K. & Blair, D. Chemotaxis signaling protein CheY binds
660 to the rotor protein FliN to control the direction of flagellar rotation in
661 *Escherichia coli*. *Proc. Natl. Acad. Sci. U.S.A.* **107,** 9370–9375 (2010).
662 14. Mathews, M. A. A., Tang, H. L. & Blair, D. F. Domain analysis of the FliM
663 protein of *Escherichia coli*. *J. Bacteriol.* **180,** 5580–5590 (1998).
664 15. Barak, R. & Eisenbach, M. Correlation between phosphorylation of the
665 chemotaxis protein CheY and its activity at the flagellar motor.
666 *Biochemistry (USA)* **31,** 1821–1826 (1992).
667 16. McEvoy, M., Bren, A., Eisenbach, M. & Dahlquist, F. W. Identification of the
668 binding interfaces on CheY for two of its targets, the phosphatase CheZ
669 and the flagellar switch protein FliM. *J. Mol. Biol.* **289,** 1423–1433 (1999).
670 17. Dyer, C. M., Vartanian, A. S., Zhou, H. & Dahlquist, F. W. A molecular
671 mechanism of bacterial flagellar motor switching. *J. Mol. Biol.* **388,** 71–84
672 (2009).
673 18. Cluzel, P., Surette, M. & Leibler, S. An ultrasensitive bacterial motor
674 revealed by monitoring signaling proteins in single cells. *Science* **287,**
675 1652–1655 (2000).
676 19. Sagi, Y., Khan, S. & Eisenbach, M. Binding of the chemotaxis response
677 regulator CheY to the isolated, intact switch complex of the bacterial
678 flagellar motor: Lack of cooperativity. *J. Biol. Chem.* **278,** 25867–25871
679 (2003).
680 20. Sourjik, V. & Berg, H. C. Binding of the *Escherichia coli* response regulator
681 CheY to its target measured *in vivo* by fluorescence resonance energy
682 transfer. *Proc. Natl. Acad. Sci. U.S.A.* **99,** 12669–12674 (2002).

683 21. Berg, H. C. & Brown, D. A. Chemotaxis inEscherichia colianalysed by
684 three-dimensional tracking. *Nature* **239,** 500–504 (1972).
685 22. Turner, L., Ryu, W. S. & Berg, H. C. Real-time imaging of fluorescent
686 flagellar filaments. *J. Bacteriol.* **182,** 2793–2801 (2000).
687 23. Vladimirov, N., Lebiedz, D. & Sourjik, V. Predicted auxiliary navigation
688 mechanism of peritrichously flagellated chemotactic bacteria. *PLoS*
689 *computational biology* **6,** e1000717 (2010).
690 24. Saragosti, J. *et al.* Directional persistence of chemotactic bacteria in a
691 traveling concentration wave. *Proc. Natl. Acad. Sci. U.S.A.* **108,** 16235–
692 16240 (2011).
693 25. Kihara, M. & Macnab, R. M. Cytoplasmic pH mediates pH taxis and weak-
694 acid repellent taxis of bacteria. *J. Bacteriol.* **145,** 1209–1221 (1981).
695 26. Repaske, D. R. & Adler, J. Change in intracellular pH of *Escherichia coli*
696 mediates the chemotactic response to certain attractants and repellents. *J.*
697 *Bacteriol.* **145,** 1196–1208 (1981).
698 27. Dyer, C. M. & Dahlquist, F. W. Switched or not?: the structure of
699 unphosphorylated CheY bound to the N terminus of FliM. *J. Bacteriol.* **188,**
700 7354–7363 (2006).
701 28. Schuster, M., Silversmith, R. E. & Bourret, R. B. Conformational coupling in
702 the chemotaxis response regulator CheY. *Proc. Natl. Acad. Sci. U.S.A.* **98,**
703 6003–6008 (2001).
704 29. de Diego Puente, T. *et al.* The Protein Acetyltransferase PatZ from
705 Escherichia coli Is Regulated by Autoacetylation-induced Oligomerization.
706 *J. Biol. Chem.* **290,** 23077–23093 (2015).
707 30. Barak, R. & Eisenbach, M. Chemotactic-like response of *Escherichia coli*
708 cells lacking the known chemotaxis machinery but containing
709 overexpressed CheY. *Mol. Microbiol.* **31,** 1125–1137 (1999).
710 31. Bourret, R. B., Hess, J. F. & Simon, M. I. Conserved aspartate residues
711 and phosphorylation in signal transduction by the chemotaxis protein
712 CheY. *Proc. Natl. Acad. Sci. U.S.A.* **87,** 41–45 (1990).
713 32. Kentner, D. & Sourjik, V. Dynamic map of protein interactions in
714 theEscherichia colichemotaxis pathway. *Mol Syst Biol* **5,** 238 (2009).
715 33. Scharf, B. E., Fahrner, K. A., Turner, L. & Berg, H. C. Control of direction of
716 flagellar rotation in bacterial chemotaxis. *Proc. Natl. Acad. Sci. U.S.A.* **95,**
717 201–206 (1998).
718 34. Saragosti, J., Silberzan, P. & Buguin, A. Modeling E. coli tumbles by
719 rotational diffusion. Implications for chemotaxis. *PLoS ONE* **7,** e35412
720 (2012).
721 35. Fraiberg, M. *et al.* CheY's acetylation sites responsible for generating
722 clockwise flagellar rotation in *Escherichia coli*. *Mol. Microbiol.* **95,** 231–244
723 (2015).
724 36. Bai, F. *et al.* Conformational spread as a mechanism for cooperativity in the
725 bacterial flagellar switch. *Science* **327,** 685–689 (2010).
726 37. Di Paolo, D., Afanzar, O., Armitage, J. P. & Berry, R. M. Single-molecule
727 imaging of electroporated dye-labelled CheY in live Escherichia coli.

Philosophical Transactions of the Royal Society of London Series B - Biological Sciences **371,** 20150492 (2016).

38. Schuster, M., Zhao, R., Bourret, R. B. & Collins, E. J. Correlated switch binding and signaling in bacterial chemotaxis. *J. Biol. Chem.* **275,** 19752–19758 (2000).
39. Liarzi, O. *et al.* Acetylation represses the binding of CheY to its target proteins. *Mol. Microbiol.* **76,** 932–943 (2010).
40. Paul, K., Brunstetter, D., Titen, S. & Blair, D. F. A molecular mechanism of direction switching in the flagellar motor of *Escherichia coli*. *Proc. Natl. Acad. Sci. U.S.A.* **108,** 17171–17176 (2011).
41. Delalez, N. J. *et al.* Signal-dependent turnover of the bacterial flagellar switch protein FliM. *Proc. Natl. Acad. Sci. U.S.A.* **107,** 11347–11351 (2010).
42. Philippe, N., Alcaraz, J.-P., Coursange, E., Geiselmann, J. & Schneider, D. Improvement of pCVD442, a suicide plasmid for gene allele exchange in bacteria. *Plasmid* **51,** 246–255 (2004).
43. Silverman, M. & Simon, M. Flagellar rotation and the mechanism of bacterial motility. *Nature* **249,** 73–74 (1974).
44. Thomas, D. R., Francis, N. R., Xu, C. & DeRosier, D. J. The three-dimensional structure of the flagellar rotor from a clockwise-locked mutant ofSalmonella entericaserovar Typhimurium. *J. Bacteriol.* **188,** 7039–7048 (2006).
45. Goldbeter, A. & Koshland, D. E. An amplified sensitivity arising from covalent modification in biological systems. *Proc. Natl. Acad. Sci. U.S.A.* **78,** 6840–6844 (1981).

Acknowledgments

We are indebted to Dr. David Blair and Paige Wheatley in his group for numerous extensive discussions, for critical reading of earlier versions of the manuscript, for disclosing their unpublished data, and for preparing some of the mutants used in this study. We thank Dr. James E. Ferrell for his contribution in the construction of the mathematical model, Dr. Ady Vaknin and Vered Frank in his group for their useful suggestions and technical assistance, Dr. S. Roy Caplan for helpful discussions, Vladimir Kiss for assistance with operating the confocal microscope, Dr. Judith Armitage for supplying bacterial strains, and Yana Gurevich for technical assistance. This study was supported by grant no. 2013197 from the US-Israel Binational Science Foundation and by grant no. 66/14 from the Israel Science Foundation to M.E., by a UK BBSRC grant no. BB/H01795X/1 and an ERC Starter grant no. ERC 261227 to A.N.K., and by a BBSRC grant to R.M.B. D.D.P. was supported by a UK EPSRC DTC studentship. A.P. was supported by a UK EPSRC DTA studentship and the German National Academic Foundation (Studienstiftung)

769 and the Phizackerley Senior Scholarship in Medical Sciences at Balliol College,
770 Oxford. O.A. was supported by an EMBO short term travel fellowship to Oxford.
771

Figures

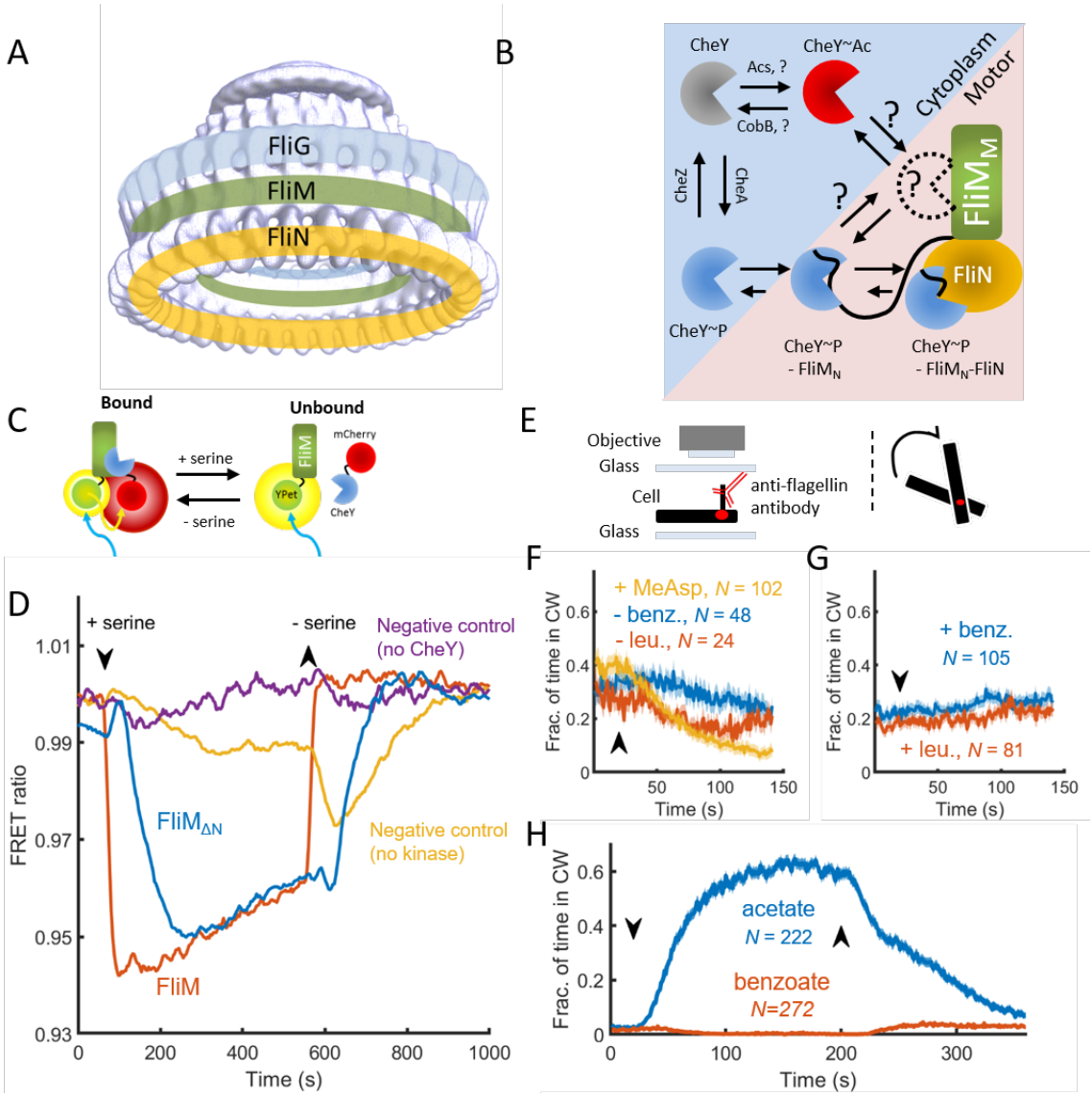

Figure 1. CheY binds to low-affinity sites at the motor to produce clockwise rotation. **A**, An electron density map of the switch complex of the flagellar motor of *Salmonella*, a relative of *E. coli*, that demonstrates the organization within the switch. The map was produced by [44] and downloaded from http://dx.doi.org/10.1093/nar/gkv1126. **B**, CheY interactions. **C**, Experimental scheme of the FRET experiment. When CheY-mCherry is in proximity to FliM-YPet, there is energy transfer from the excited YPet fluorophore to mCherry, as a result of which excitation of YPet results in red fluorescence of mCherry. The attractant serine lowers the phosphorylation level of CheY with a consequent dissociation from FliM. Therefore, following attractant addition, FRET is reduced and excitation of YPet results in yellow emission typical of YPet fluorescence. **D**, Representative FRET measurements of cells in response to an attractant stimulus

786 (0.1 mM serine). (See Figure S1 for the detailed analysis and Figure S2 for other
787 measurements.) FRET ratio is the ratio of mCherry to YPet fluorescence. CheY-
788 mCherry and mCherry concentrations were ~170 μM in the case of $FliM_{\Delta N}$ and ~15
789 μM in the case of wild-type FliM (Figure S3A for calibration of CheY concentration).
790 Data were smoothed with a mean window at the size of 10 data points. **E**,
791 Experimental scheme for measurement of tethered motors: Motors (red point) are
792 tethered to glass in a flow chamber *via* anti-flagellin antibody (red). When observed
793 from above, the direction of cell rotation indicates the direction of motor rotation.
794 **F**, The response of tethered *fliM*$_{\Delta N}$ Δ*cheZ* cells (strain EW635), induced for CheY
795 expression from a plasmid (200 μM IPTG), to positive chemotactic stimulation.
796 Lines and shaded regions of the average fraction of time spent in clockwise rotation
797 are the mean ± SEM. The arrow shows the time of stimulation. N is the number of
798 cells. MeAsp and leucine were used at 1 mM, benzoate (pH 7.0) at 50 mM. **G**, As
799 in F, but for negative chemotactic stimulation. **H**, Response of tethered *fliM*$_{\Delta N}$ cells
800 (strain sPW416), induced for CheY expression from a plasmid (800 μM IPTG), to
801 acetate and benzoate (both at 50 mM, pH 7.0). Lines and shaded regions of the
802 average fraction of time spent in clockwise rotation are the mean ± SEM. Down-
803 and up-arrows mark the introduction and the removal of stimuli, respectively.

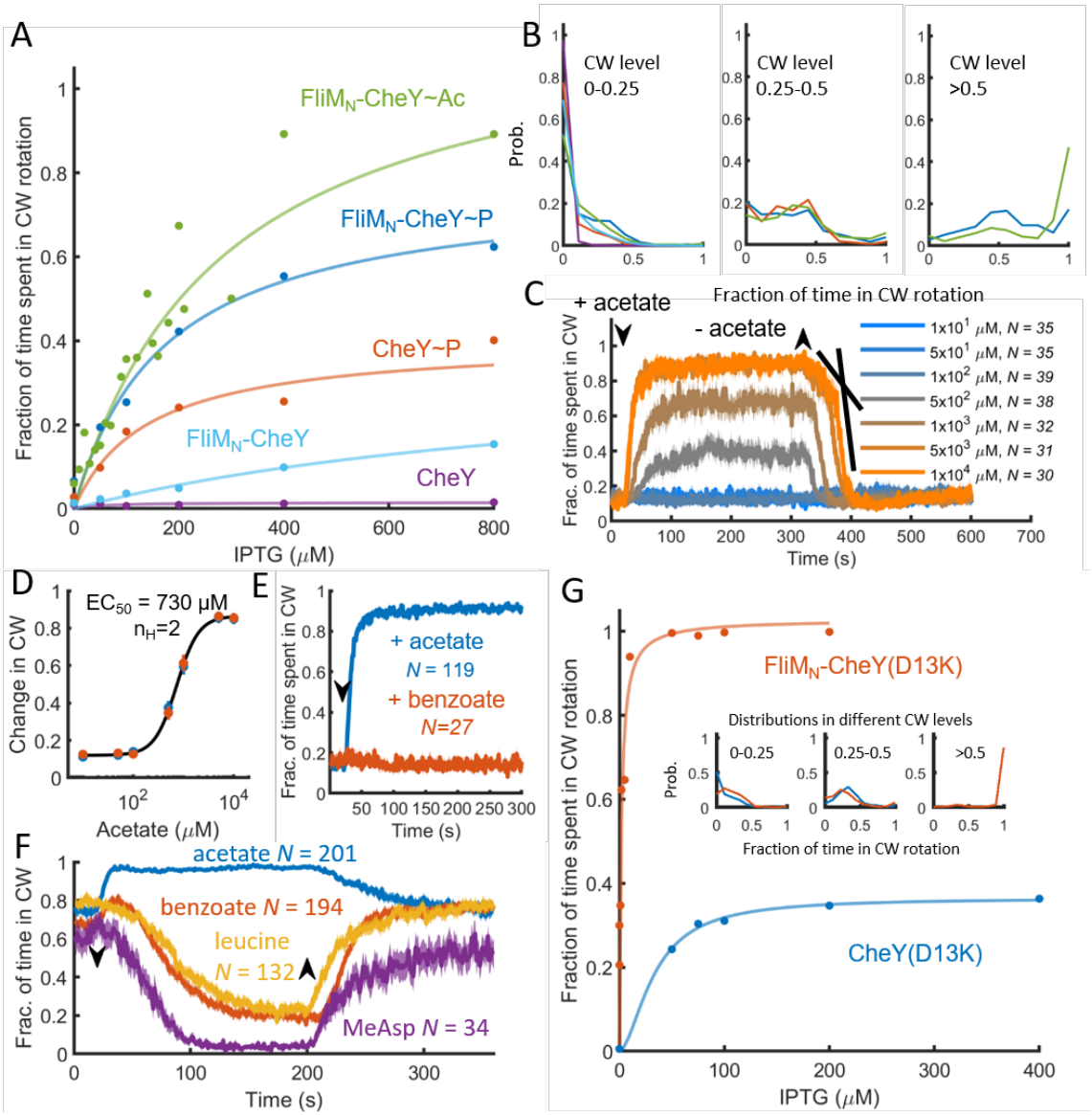

Figure 2. FliM$_N$ is an activator of CheY. **A**, Dependence of clockwise rotation on the levels of CheY~P and FliM$_N$-CheY~P. The figure shows the mean of clockwise rotation in tethered *fliM*$_{\Delta N}$ Δ*cheZ* cells expressing CheY (red) or FliM$_N$-CheY (blue; strains EW694 and EW697, respectively) and *fliM*$_{\Delta N}$ Δ*cheA* cells expressing CheY (purple) or FliM$_N$-CheY (cyan; strains EW693 and EW696, respectively), with IPTG as an inducer. For FliM$_N$-CheY~Ac (green), acetate (10 mM, pH 7.0) was employed. Each data point is the average of all measurements at a given IPTG concentration, weighted by the sample number of each experiment. For data, see Table S1. **B**, Distributions of the data in A. **C**, Mean response of *fliM*$_{\Delta N}$ Δ*cheA* cells expressing FliM$_N$-CheY (EW696) to introduction or removal of varying acetate concentrations (pH 7.0). FliM$_N$-CheY expression was induced with 800 μM IPTG. Black lines mark the apparent biphasic response to acetate removal. N is the number of cells. **D**, Changes in clockwise rotation induced by acetate, calculated

818 from C as the difference in clockwise levels between time segments 0-20 s and
819 280-300 s (stimulus introduction; red) or between time segments 580-600 s and
820 300-320 s (stimulus removal; blue). Black line is a Hill fit. **E**, Comparison of the
821 mean response of cells to acetate and benzoate. Details as in C, but different cells
822 were examined. Acetate and benzoate at 10 mM (pH 7.0). **F**, Mean response of
823 *fliM*$_{\Delta N}$ cells expressing FliM$_N$-CheY (sPW417) to the introduction or removal of
824 acetate, benzoate (each at 50 mM, pH 7.0), leucine and MeAsp (each at 1 mM).
825 FliM$_N$-CheY expression was induced with 800 μM IPTG. **G**, Dependence of
826 clockwise rotation on the levels of CheY(D13K) and FliM$_N$-CheY(D13K). As in A-B
827 for tethered *fliM*$_{\Delta N}$ Δ*cheA* cells expressing CheY(D13K) or FliM$_N$-CheY(D13K)
828 (strains EW737 and EW739, respectively).

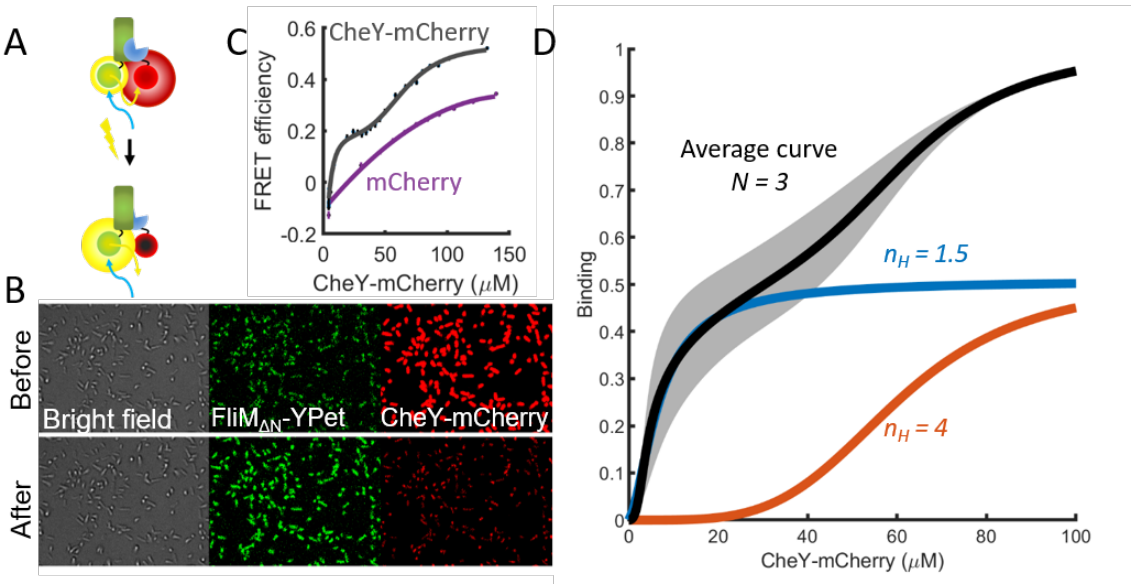

829

830 **Figure 3**. CheY binding to the motor is biphasic. **A**, Experimental scheme: the ratio
831 of YPet fluorescence before and after mCherry photobleaching indicates the extent
832 of CheY binding by FliM$_{\Delta N}$. **B**, Demonstration of FRET acquisition, showing the
833 enhancement of FliM$_{\Delta N}$-YPet fluorescence due to mCherry photobleaching. **C**, One
834 representative experiment out of 3 (black points and curve). Purple data points and
835 curves show a control performed in parallel with free mCherry. FRET efficiency
836 was calculated as the ratio of yPET fluorescence before and after photobleaching
837 of mCherry. The data points are the mean ± SEM of 100 observations each. Curve
838 is a fit to a double Hill expression (n_{H1} = 2, n_{H2} = 4). **D**, FRET response curve as a
839 function of the CheY-mCherry concentration. Black curve is the average fit of three
840 different normalized experiments to a double-Hill expression; shaded region is ±
841 SEM. Red and blue curves were derived from the black curve. The conversion of
842 mCherry fluorescence intensity to CheY concentration was estimated according to
843 Figure S3B-C.

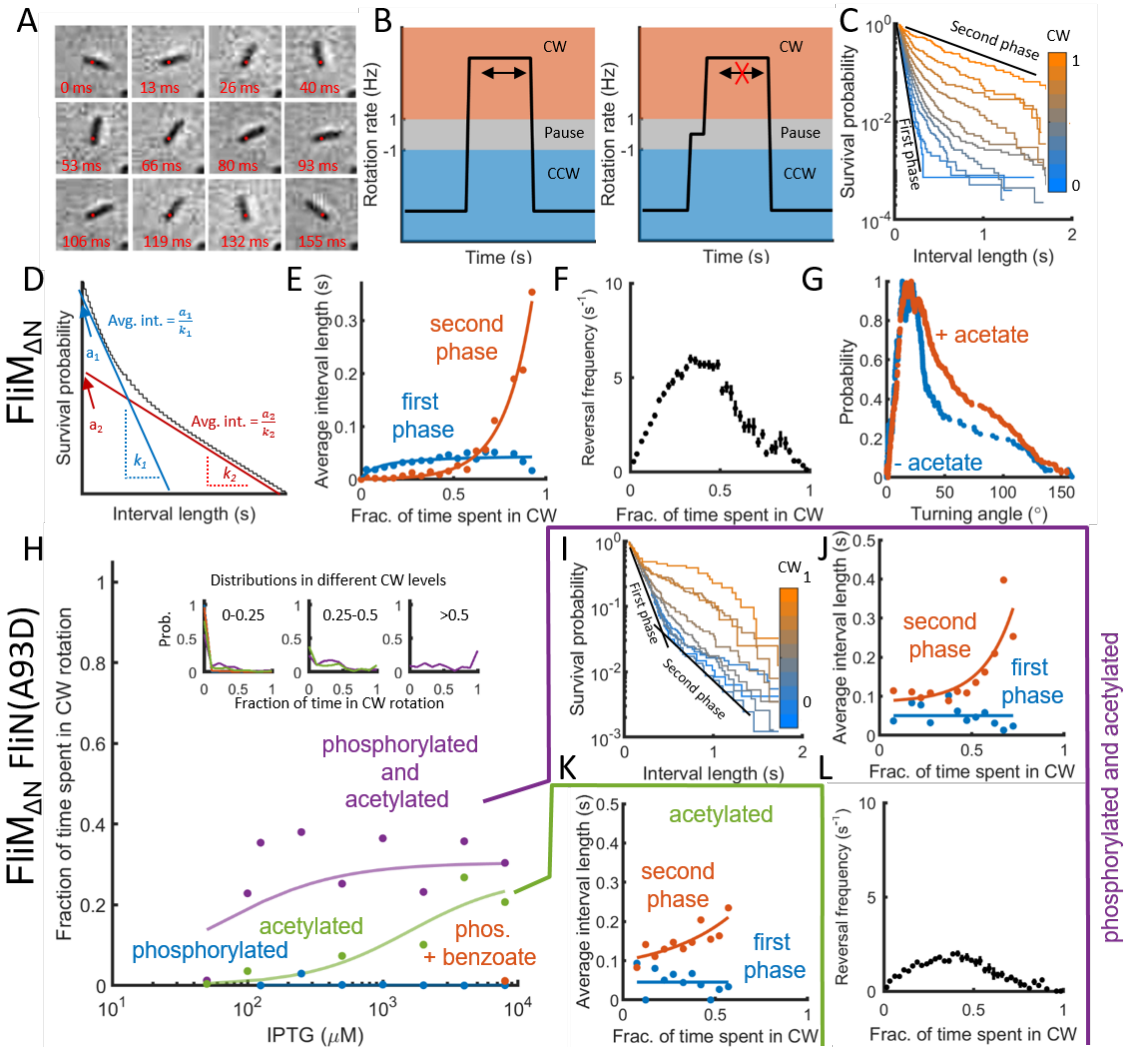

Figure 4. Clockwise generation is a biphasic process initiated by CheY binding to FliN. **A**, A demonstration of clockwise interval measurement. Red points, axes of rotation; black, the cell body. Clockwise rotation is apparent between ~50 and 90 ms. **B**, Demonstration of clockwise intervals considered valid and invalid (left and right, respectively). **C**, Distribution of clockwise interval lengths at different average clockwise levels in Δ*cheA* cells containing FliM$_{\Delta N}$ motors and expressing FliM$_N$-CheY (strain EW696), in the presence of acetate (10 mM, pH 7.0). Color gradient changes in 0.1 steps from 0 to 1 clockwise rotation. The black lines show the distributions associated with the first and second phases. **D**, Demonstration of a calculation of clockwise rotation time of each phase at each clockwise level. Distributions as in D were fitted with a biexponential decay expression. In each distribution and for each phase of exponential decay, the average interval length was calculated as the exponential pre-factor divided by the decay rate. **E**, Average interval length in each of the phases as a function of clockwise level for the distributions in C. **F**, Average reversal frequency as a function of clockwise level.

860 Same cells shown in C. **G**, Small deflection angles of swimming in cells that exhibit
861 mostly a single switching phase. The distributions shown herein are the angle
862 deflection distributions of free-swimming cells in Figure S6, after subtracting the
863 control distributions of cells that do not express CheY (in which deflection angles
864 represent noise). For clarity, the distributions were normalized according to the
865 maximal value of the distribution. The experimental cells were Δ*cheA* containing
866 $FliM_{\Delta N}$ motors and expressing $FliM_N$-CheY (strain EW696). The control cells were
867 Δ*cheY* (strain UU1631). The measurements were performed in the presence and
868 absence of acetate (10 mM, pH 7.0). **H**, Effects of $FliM_N$-CheY acetylation and
869 phosphorylation on clockwise rotation of tethered cells containing $FliM_{\Delta N}$
870 FliN(A93D) motors. Acetate and benzoate concentrations were 10 mM each (pH
871 7.0). Non-phosphorylated and phosphorylated CheY was produced by using
872 Δ*cheA* and Δ*cheZ* backgrounds (strains EW713 and EW714, respectively). Each
873 data point is the average of all measurements at a given IPTG concentration,
874 weighted by the sample number of each experiment. Distributions were drawn with
875 respect to experiments with same range of average clockwise rotation. For data
876 see Table S1. **I-L**, As in C, E, F, except that in I, J, L the cells used were Δ*cheZ* (I,
877 J, L) or Δ*cheA* (K) containing $FliM_{\Delta N}$ FliN(A93D) motors and expressing $FliM_N$-
878 CheY (strain EW714 or EW713, respectively).

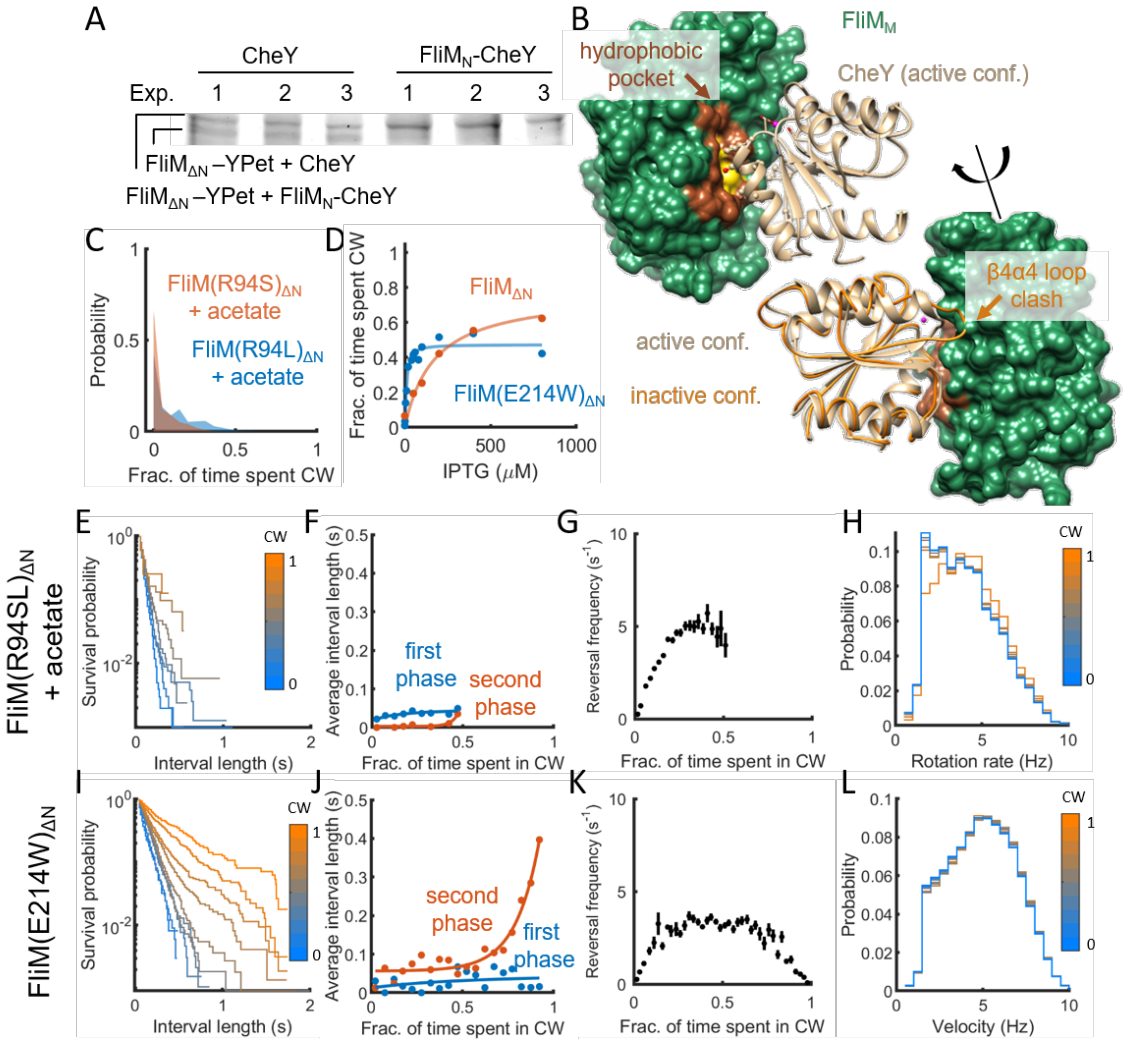

Figure 5. The second switching phase is associated with CheY binding to $FliM_M$. **A**, CheY crosslinks with $FliM_{\Delta N}$-YPet. Cells overexpressing CheY or $FliM_N$-CheY from a plasmid were crosslinked with glutaraldehyde. The cytoplasm of the cells was resolved by SDS-PAGE. The gel was imaged for $FliM_{\Delta N}$-YPet fluorescence. The figure shows a gel where three different samples of CheY and $FliM_N$-CheY were resolved. Full details as in Figure S7. **B**, Docking simulation between the predicted binding interfaces of CheY and $FliM_M$ in *E. coli*. The solvent accessible surface of $FliM_M$ is shown in green, with a binding depression area and its surrounding ridge highlighted in yellow and brown, respectively. **Up-left**, The predicted interaction of activated CheY with $FliM_M$ in *E. coli*. CheY is depicted as a beige ribbon, with residues shown as ball and stick corresponding to the interacting residues in *T. maritima*. Mg^{2+} ions are shown as magenta spheres. **Down-right**, The active form of the β4α4 loop of CheY is predicted to promote CheY interaction with $FliM_M$. The predicted CheY-$FliM_M$ complex in *E. coli* rotated by approximately 180° about the vertical axis aligned with the inactivated conformation of CheY

895 (orange coil). The region in the inactivated conformation that clashes with $FliM_M$
896 was previously predicted to acquire an active conformation in the case of
897 CheY(K91) acetylation [35]. **C**, Clockwise rotation of tethered *fliM(R94S)*$_{\Delta N}$ Δ*cheZ*
898 cells or *fliM(R94L)*$_{\Delta N}$ Δ*cheZ* cells (strain EW731 or EW733, respectively)
899 expressing $FliM_N$-CheY in the presence of acetate (10 mM, pH 7.0). $FliM_N$-CheY
900 expression was induced by 8 mM IPTG. For data see Table S1. **D**, Clockwise
901 rotation of tethered *fliM*(E214W)$_{\Delta N}$ Δ*cheZ* cells at various levels of IPTG for the
902 induction of $FliM_N$-CheY expression. Each data point is the average of all
903 measurements at similar IPTG concentration, weighted by the sample number of
904 each experiment. For data see Table S1. **E**, The distribution of clockwise intervals
905 for *fliM(R94SL)*$_{\Delta N}$ Δ*cheZ* cells expressing $FliM_N$-CheY in the presence of acetate
906 (10 mM, pH 7). **F**, Average interval length in each of the phases as a function of
907 clockwise level for the distributions in E. **G***,* Average reversal frequency as a
908 function of clockwise level. Same cells shown in E. **H,** A histogram of clockwise
909 rotation velocities at different clockwise levels. Same cells shown in E. **I-L**, Same
910 as E-H, except that cells of *fliM*(E214W)$_{\Delta N}$ Δ*cheZ* expressing $FliM_N$-CheY were
911 used in the absence of acetate.

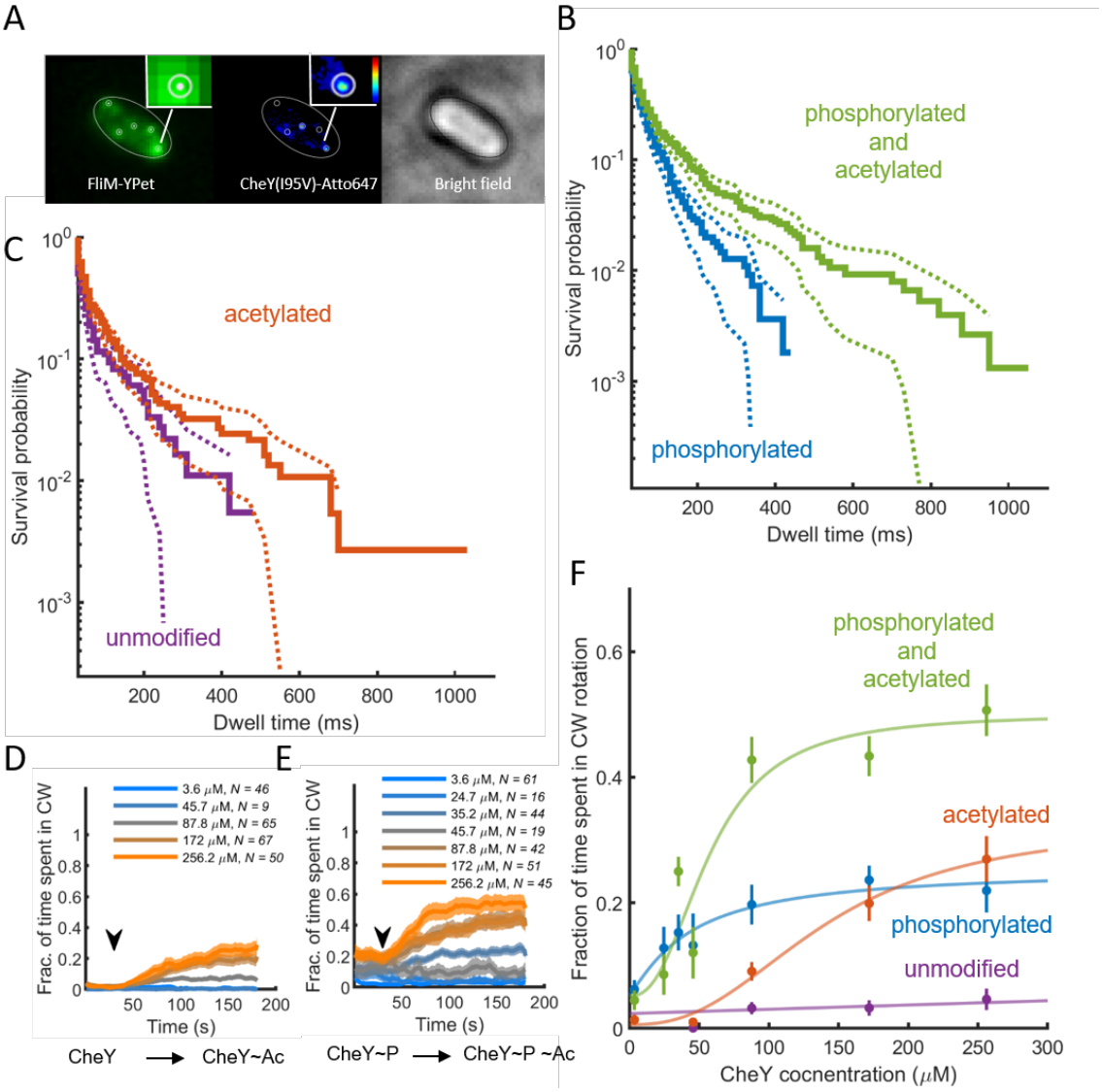

Figure 6. CheY~Ac and CheY~P differ in their effective concentration and motor binding kinetics. **A**, Demonstration of single-molecule tracking in a single cell. Left, Imaged FliM-YPet fluorescence. White dots indicate the estimated motor locations. White circles illustrate a 75 nm radius around these locations. Middle, Contour map of the normalized sum of probabilities of the localization events of CheY(I95V)-Atto647 (from blue to red is low to high; black is zero probability). White circles show motor locations from the left panel. Right, Bright-field image of the cell. **B**, Survival probabilities phosphorylated CheY(I95V)-Atto647 at the motor under acetylating and non-acetylating conditions (presence or absence of acetate [50 mM, pH 7.0], green and blue, respectively). CheY was mostly phosphorylated due to the Δ*cheZ* background (strain EW669). Dashed lines are confidence bounds of the distribution at 95%. The number of cells recorded was 82 and 40 (without and with acetate, respectively). The number of trajectories in which CheY was found to

interact with FliM was 2414 and 2660 (without and with acetate). **C**, As in B for a Δ*cheA* background (strain EW668). The number of cells recorded was 63 and 56 (without and with acetate). The number of trajectories in which CheY was found to interact with FliM was 1316 and 1904 (without and with acetate). **D**, Response of tethered *fliM*$_{\Delta N}$ Δ*cheA* cells (strain EW634) to acetate (50 mM, pH 7.0) at different CheY concentrations. Lines and shaded regions are mean ± SEM. **E**, Response of tethered *fliM*$_{\Delta N}$ Δ*cheZ* cells (strain EW635) to acetate. Details as in D. **F**, Contribution of acetylation and phosphorylation to switching to clockwise rotation. The points are the mean clockwise rotation calculated from D, E at time segments 0-20 s and 160-180 s.

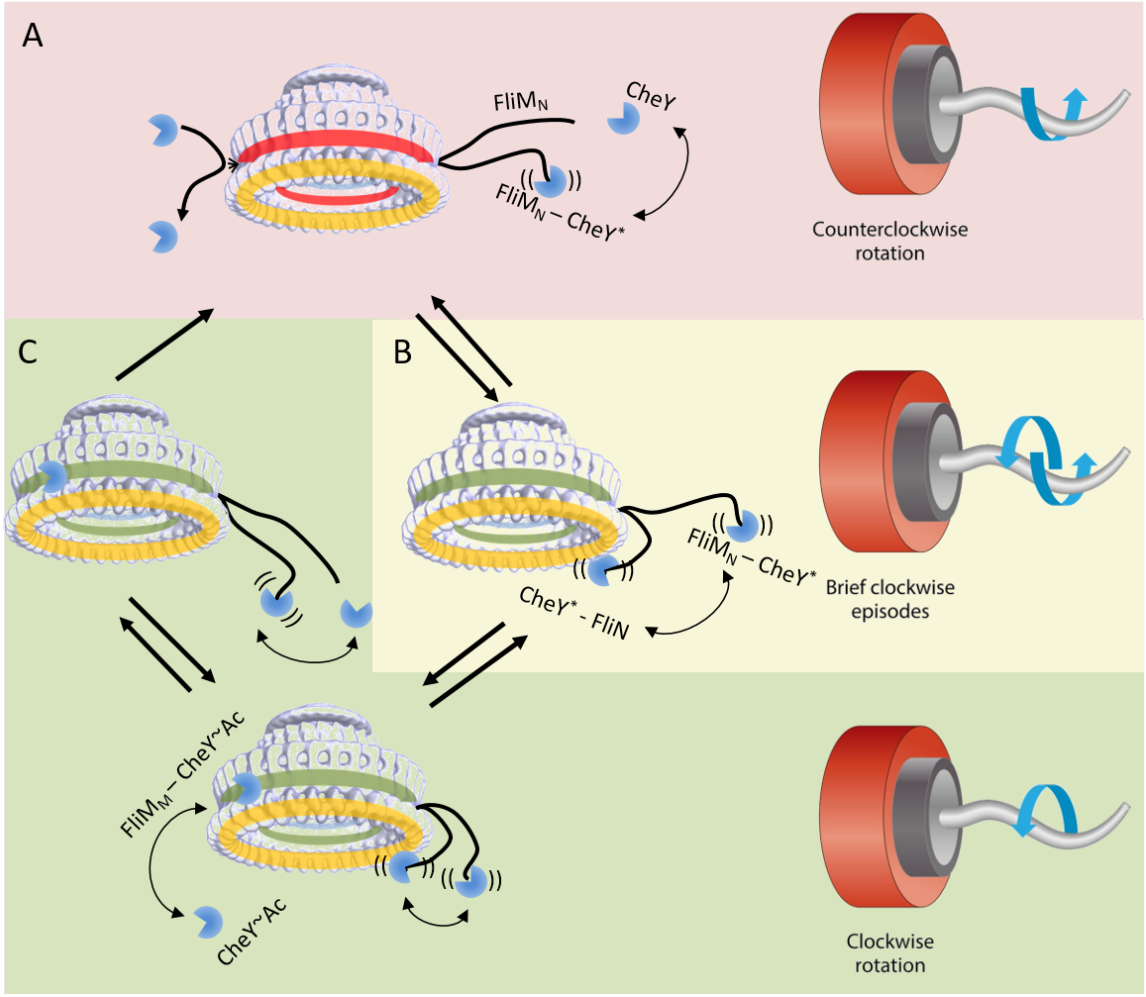

Figure 7. A model for clockwise generation by CheY~P and CheY~Ac. The model suggests the most likely interactions of CheY at the motor. Yellow motor ring, FliN. Red motor ring, FliM in a conformation that cannot bind CheY. Green motor ring, FliM in a conformation that can bind CheY. Red background region is counterclockwise rotation. Yellow background region is frequent switching. Green shaded region is consecutive clockwise rotation. See text for details.

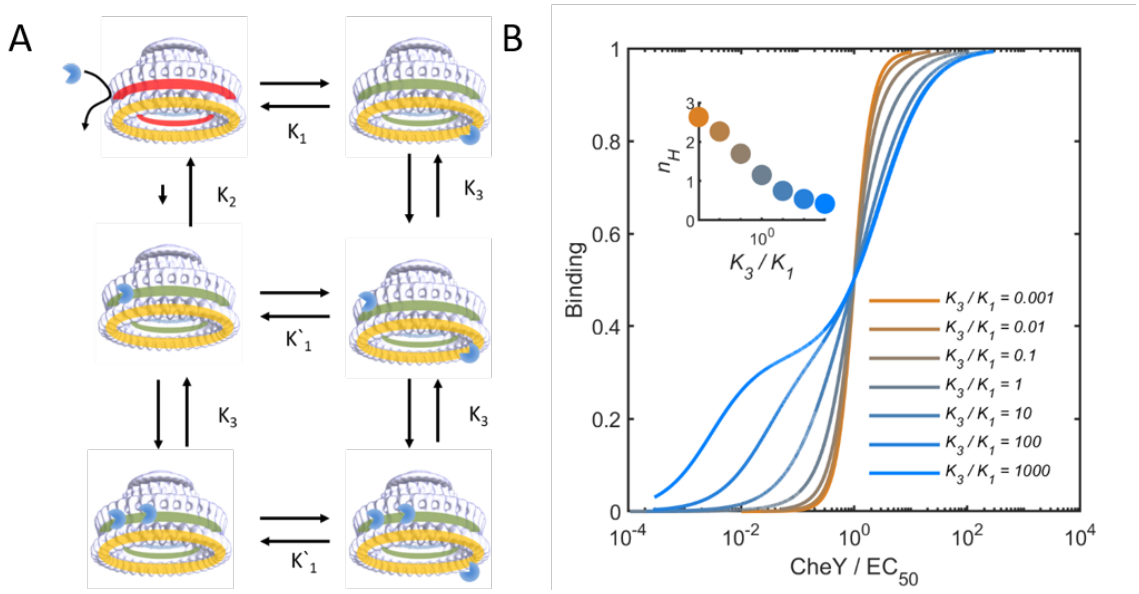

Figure 8. Kinetic model demonstrates varying levels of ultrasensitivity produced by a gateway system. **A**, The kinetic model. Yellow ring represents CheY binding site at FliN. The ring at the middle of the motor represents CheY binding sites in $FliM_M$, when the motor is rotating counterclockwise (red) or clockwise (green). **B**, Binding curve solution of the kinetic model for different K_3 values (binding to both FliN and $FliM_M$). K_1 was set as 1. K_2 was set as 10^6 K_1. Different colors are solutions for different K_3 values. Ligand levels were normalized to half-saturation point (EC_{50}) of each curve. Note that normalized ligand concentrations are shown in log-scale. The solution of the model was generated in Mathematica. ***Insert***, Calculated apparent Hill-coefficient for the curves in the main panel. Apparent Hill-coefficient was calculated as $\log_{10}(81)/\log_{10}(EC_{90}/EC_{10})$ [45].